molecular pharmaceutics

brief articles

Growth of Itraconazole Nanofibers in Supersaturated Simulated Intestinal Fluid

Randy Mellaerts,[†] Alexander Aerts,[†] Tom P. Caremans,[†] Jan Vermant,[‡] Guy Van den Mooter,[§] Johan A. Martens,*[,†] and Patrick Augustijns[§]

Centre for Surface Chemistry and Catalysis, Laboratory for Pharmacotechnology and Biopharmacy, and Laboratory of Applied Rheology and Polymer Technology, K. U. Leuven, Belgium

Received December 2, 2009; Revised Manuscript Received March 6, 2010; Accepted March 16, 2010

Abstract: Many drug compounds have limited solubility in water. To enhance the oral bioavailability of such compounds, pharmaceutical formulations target the creation of a supersaturated solution. Release of the compound from ordered mesoporous silica carrier is such a means for reaching supersaturation. Little is known about the evolution of supersaturated intestinal media. The present study reveals the phase transitions of the poorly water-soluble drug itraconazole in simulated intestinal fluid under conditions corresponding to supersaturation. Electron spin resonance of *n*-doxylstearic acid spin probes evidenced that during supersaturation itraconazole is solubilized inside the hydrophobic core of mixed micelles composed of lecithin and bile salt. Cryogenic transmission electron microscopy revealed that the supersaturated state of itraconazole provokes the formation of nanofibers with a uniform diameter of 12 nm. The nanofiber length determined via dynamic light scattering increases from 220 to 1480 nm after 30 and 90 min, respectively. Nanofibers drastically reduced transepithelial transport of itraconazole across a Caco-2 cell monolayer mimicking the gastrointestinal absorption. Based on our study, we suggest the existence of an optimum intraluminal itraconazole supersaturation at which itraconazole absorption is enhanced but formation of itraconazole nanofibers prevented.

Keywords: Supersaturation; SBA-15; drug delivery; micelles; itraconazole

Introduction

Many potential drug candidates as identified using combinatorial research and selected from biologically based high-throughput screening are poorly soluble in water.[1] Oral administration of such poorly water-soluble drugs is often inefficient because of insufficient dissolution of the compound in the gastrointestinal fluids.[2] Pharmaceutical formulation of such compounds is oriented toward the creation of a supersaturated solution upon contact with aqueous environment. A supersaturating drug delivery system (SDDS) generates a solution of a poorly water-soluble drug that exceeds the thermodynamic equilibrium concentration within the intraluminal environment. Enhanced absorption can be expected provided such increased drug concentrations are maintained during a sufficient time period.[3] Methods and strategies for the development of SDDS have recently been

* Corresponding author. Tel: (+32) 16 321637. Fax: (+32) 16 321998. E-mail: johan.martens@biw.kuleuven.be. Centre for Surface Chemistry and Catalysis, Kasteelpark Arenberg 23, Katholieke Universiteit Leuven, BE-3001 Heverlee, Belgium.

[†] Centre for Surface Chemistry and Catalysis.

[‡] Laboratory of Applied Rheology and Polymer Technology.

[§] Laboratory for Pharmacotechnology and Biopharmacy.

(1) Report by Technology Catalysts International Corporation, Delivery of Poorly Soluble Drugs, Falls Church, VA, 3rd ed., 2002.

(2) Rabinow, B. E. Nanosuspensions in drug delivery. *Nat. Rev. Drug Discovery* **2004**, *3*, 785–796.

(3) Vandecruys, R.; Peeters, J.; Verreck, G.; Brewster, M. E. Use of a screening method to determine excipients which optimize the extent and stability of supersaturated drug solutions and application of this system to solid formulation design. *Int. J. Pharm.* **2007**, *342*, 168–175.

10.1021/mp900300j
Published on Web 03/16/2010

reviewed by Brouwers et al.[4] A thermodynamically unstable, supersaturated solution of a drug can only be generated starting from the drug molecule at a higher energy level as compared to the crystalline state.[5] Formulation strategies to reach supersaturation in the gastrointestinal lumen include the use of cosolvents,[6] lipid-based formulations,[7] and solid dispersions[8] and release of the drugs from mesoporous silica adsorbents.[9]

Itraconazole is a triazole antimycotic drug with extremely low aqueous solubility of 4 $\mu g \cdot mL^{-1}$ at pH 1 and less than 1 $ng \cdot mL^{-1}$ at neutral pH.[10] It often is used as a model drug compound during evaluation of the potential of an SDDS. It became available on the market in 1986 formulated as a molecular dispersion in an amorphous hydroxypropylmethylcellulose phase coated onto sugar beads (Sporanox). With the introduction of cyclodextrins as complexing agents, itraconazole became available as an oral solution.[11] The enhanced oral bioavailability of itraconazole was demonstrated to correlate with the degree of supersaturation achieved after acid to neutral pH transition.[12] Release of itraconazole from ordered mesoporous silica material generates a supersaturated state in fasted state simulated intestinal fluid (FaSSIF).[13] The large internal surface area of these silicates serves the adsorption and subsequent release of guest molecules such as therapeutic active drugs. Besides the SDDS application, ordered mesoporous silica have been exploited to obtain a sustained drug release based on the hindered diffusion inside the mesopores.[14] Release can also be triggered by external stimuli when the mesopores are capped with magnetic or pH sensitive gatekeepers.[15] Downsizing the particles and controlling their morphology into the nanometer range has provided drug cargo systems that are suited for cellular uptake and subsequent release of drug molecules. These systems present a promising delivery

(4) Brouwers, J.; Brewster, M. E.; Augustijns, P. Supersaturating Drug Delivery Systems: The Answer to Solubility-Limited Oral Bioavailability. *J. Pharm. Sci.* **2009**, *89*, 2549–2572.

(5) Matteucci, M. E.; Miller, M. A.; Williams, R. O., III; Johnston, K. P. Highly Supersaturated Solutions of Amorphous Drugs Approaching Predictions from Configurational Thermodynamic Properties. *J. Phys. Chem. B* **2008**, *112*, 16675–16681.

(6) (a) Urbanetz, N. A. Stabilization of solid dispersions of nimodipine and polyethylene glycol 2000. *Eur. J. Pharm. Sci.* **2006**, *28*, 67–76. (b) Murnane, D.; Marriott, C.; Martin, G. P. Comparison of salmeterol xinafoate microparticle production by conventional and novel antisolvent crystallization. *Eur. J. Pharm. Biopharm.* **2008**, *69*, 94–105. (c) Goddeeris, C.; Van den Mooter, G. Free flowing solid dispersions of the anti-HIV drug UC 781 with Poloxamer 407 and a maximum amount of TPGS 1000: Investigating the relationship between physicochemical characteristics and dissolution behaviour. *Eur. J. Pharm. Sci.* **2008**, *35*, 104–113.

(7) (a) O'Driscoll, C. M.; Griffin, B. T. Biopharmaceutical challenges associated with drugs with low aqueous solubility—The potential impact of lipid-based formulations. *Adv. Drug Delivery Rev.* **2008**, *60*, 617–624. (b) Narang, A. S.; Delmarre, D.; Gao, D. Stable drug encapsulation in micelles and microemulsions. *Int. J. Pharm.* **2007**, *345*, 9–25.

(8) (a) Vasconcelos, T.; Sarmento, B.; Costa, P. Solid dispersions as strategy to improve oral bioavailability of poor water soluble drugs. *Drug Discovery Today* **2007**, *12*, 1068–1075. (b) Kennedy, M.; Hu, J.; Gao, P.; Li, L.; Ali-Reynolds, A.; Chal, B.; Gupta, V.; Ma, C.; Mahajan, N.; Akrami, A.; Surapaneni, S. Enhanced Bioavailability of a Poorly Soluble VR1 Antagonist Using an Amorphous Solid Dispersion Approach: A Case Study. *Mol. Pharmaceutics* **2008**, *5*, 981–993.

(9) (a) Van Speybroeck, M.; Barillaro, V.; Do Thi, T.; Mellaerts, R.; Martens, J. A.; Van Humbeeck, J.; Vermant, J.; Annaert, P.; Van Den Mooter, G.; Augustijns, P. Ordered Mesoporous Silica Material SBA-15: A Broad-Spectrum Formulation Platform for Poorly Soluble Drugs. *J. Pharm. Sci.* **2009**, *98*, 2648–2658. (b) Mellaerts, R.; Aerts, C. A.; Van Humbeeck, J.; Augustijns, P.; Van den Mooter, G.; Martens, J. A. Enhanced release of itraconazole from ordered mesoporous SBA-15 silica materials. *Chem. Commun.* **2007**, *13*, 1375–1377. (c) Mellaerts, R.; Mols, R.; Jammaer, J. A. G.; Aerts, C. A.; Annaert, P.; Van Humbeeck, J.; Van den Mooter, G.; Augustijns, P.; Martens, J. A. Increasing the oral bioavailability of the poorly water soluble drug itraconazole with ordered mesoporous silica. *Eur. J. Pharm. Biopharm.* **2008**, *69*, 223–230. (d) Mellaerts, R.; Jammaer, J. A. G.; Van Speybroeck, M.; Chen, H.; Van Humbeeck, J.; Augustijns, P.; Van den Mooter, G.; Martens, J. A. Physical state of poorly water soluble therapeutic molecules loaded into SBA-15 ordered mesoporous silica carriers: A case study with itraconazole and ibuprofen. *Langmuir* **2008**, *24*, 8651–8659. (e) Heikkila, T.; Salonen, J.; Tuura, J.; Kumar, N.; Salmi, T.; Murzin, D. Y.; Hamdy, M. S.; Mul, G.; Laitinen, L.; Kaukonen, A. M.; Hirvonen, J.; Lehto, V.-P. Evaluation of mesoporous TCPSi, MCM-41, SBA-15, and TUD-1 materials as API carriers for oral drug delivery. *Drug Delivery* **2007**, *14*, 337–347. (f) Ambrogi, V.; Perioli, L.; Marmottini, F.; Accorsi, O.; Pagano, C.; Ricci, M.; Rossi, C. Role of mesoporous silicates on carbamazepine dissolution rate enhancement. *Microporous Mesoporous Mater.* **2008**, *113*, 445–452.

(10) Ghazal, H. S.; Dyas, A. M.; Ford, J. L.; Hutcheon, G. A. In vitro evaluation of the dissolution behaviour of itraconazole in biorelevant media. *Int. J. Pharm.* **2009**, *366*, 117–123.

(11) Brewster, M. E.; Loftsson, T. Cyclodextrins as pharmaccutical solubilizers. *Adv. Drug Delivery Rev.* **2007**, *59*, 645–666.

(12) Miller, D. A.; DiNunzio, J. C.; Yang, W.; McGinity, J. W.; Williams, R. O., III. Enhanced in vivo absorption of itraconazole via stabilization of supersaturation following acidic-to-neutral pH transition. *Drug Dev. Ind. Pharm.* **2008**, *34*, 890–902.

(13) Mellaerts, R.; Mols, R.; Kayaert, P.; Annaert, P.; Van Humbeeck, J.; Van den Mooter, G.; Martens, J. A.; Augustijns, P. Ordered mesoporous silica induces pH-independent supersaturation of the basic low solubility compound itraconazole resulting in enhanced transepithelial transport. *Int. J. Pharm.* **2008**, *357*, 169–179.

(14) (a) Izquierdo-Barba, I.; Sousa, E.; Doadrio, J. C.; Doadrio, A. L.; Perez-Pariente, J.; Martinez, A.; Babonneau, F.; Vallet-Regi, M. Influence of mesoporous structure type on the controlled delivery of drugs: release of ibuprofen from MCM-48, SBA-15 and functionalized SBA-15. *J. Sol-Gel Sci. Technol.* **2009**, *50*, 421–429. (b) Rigby, S. P.; Fairhead, M.; van der Walle, C. F. Engineering silica particles as oral drug delivery vehicles. *Curr. Pharm. Des.* **2008**, *14*, 1821–1831. (c) Aerts, C.; Verraedt, E.; Mellaerts, R.; Depla, A.; Augustijns, P.; Van Humbeeck, J.; Van den Mooter, G.; Martens, J. A. Tunability of pore diameter and particle size of amorphous microporous silica for diffusive controlled release of drug compounds. *J. Phys. Chem. C* **2007**, *111*, 13404–13409.

(15) Angelos, S.; Johansson, E.; Stoddart, J. F.; Zink, J. I. Mesostructured silica supports for functional materials and molecular machines. *Adv. Funct. Mater.* **2007**, *17*, 2261–2271.

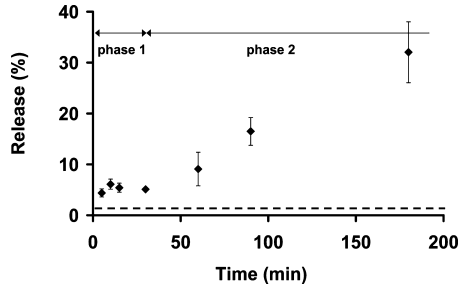

Figure 1. Itraconazole fraction released from SBA-15 in FaSSIF (pH 6.5). The total amount of itraconazole initially loaded into SBA-15 theoretically would result in a concentration of 75 μM after 100% release. Average $\pm$ SD $n = 3$. The equilibrium solubility of crystalline itraconazole in FaSSIF is presented as a dashed line (- - -). Adapted with permission from ref 13. Copyright 2008 Elsevier.

platform in the targeted treatment of cancer cells.[16] It has to be noted, however, that certain types of ordered mesoporous silica nanoparticles inhibit cellular respiration.[17]

The *in vitro* pharmaceutical performance of the ordered mesoporous silica material SBA-15 as SDDS for the release of itraconazole in FaSSIF, as adapted from earlier work,[13] is presented in Figure 1. The release process can be divided into two separate phases as indicated on the release curve. The total amount of itraconazole initially loaded into SBA-15 theoretically would result in a concentration of 75 μM after 100% release. A first part of the release curve starts at time zero and ends after ca. 30 min. During this first period, the fraction of itraconazole released into FaSSIF reaches a maximum at 6.1% after 10 min and decreases slightly to 5.1% after 30 min. Following this initial phase, the amount of itraconazole released rises quickly reaching values of 16.5 $\pm$ 2.7% and 32.0 $\pm$ 2.7% after 90 and 180 min, respectively. This second phase eventually reaches a plateau value of 73.2 $\pm$ 4.8%. This plateau value is maintained for at least three days. The thermodynamic equilibrium solubility of crystalline itraconazole corresponds to 0.40 $\pm$ 0.03 μM, and has been included in Figure 1 as a dotted line. Both phases of itraconazole release were claimed to generate itraconazole concentrations that exceed the thermodynamic equilibrium solubility of crystalline itraconazole. The second phase suggests an apparently stable state of supersaturation for at least three days. This stable supersaturation seems to be a *contradictio in terminis* as supersaturated states tend to crystallize when no precipitation inhibitors are included.[18] Using SBA-15 as SDDS with the poorly water-soluble drug itraconazole resulted in a significantly enhanced transepithelial transport in a Caco-2 system and in an *in situ* perfusion setup when comparison was made with crystalline itraconazole dissolved up to its thermodynamic equilibrium solubility in FaSSIF.[13] Itraconazole absorption from the gut takes place through passive diffusion and can be described by Fick's law. A temporary supersaturated state enhances the uptake of poorly water-soluble drugs. Very often, the pharmaceutical performance of the SDDS is investigated in complex biorelevant simulated intestinal media containing amphiphilic molecules and supramolecular assemblies such as micelles.[19] Elucidating the exact physical state of poorly water-soluble drug molecules in supersaturated intestinal media is crucial for understanding *in vitro* release and absorption profiles. The present work therefore aims to probe the physical state of supersaturated itraconazole generated with SBA-15 as SDDS in FaSSIF. A combination of cryo-TEM (cryogenic transmission electron microscopy), DLS and SLS (dynamic and static light scattering) and ESR (electron spin resonance) using spin probes was applied for detailed *in situ* investigation.

Materials and Methods

Synthesis of SBA-15. Six grams of triblock copolymer Pluronic P123 (BTC-Benelux) was dissolved in 180 g of 2 M HCl. This mixture was placed in an oil bath at 35 °C with magnetic stirring. An amount of 15.3 g of sodium silicate solution (>27 wt % SiO_2, Riedel-de Haën) was diluted with 45 g of demineralized water. This mixture was added dropwise to the Pluronic P123 solution under magnetic stirring at 500 rpm (IKA). After 24 h, the silica suspension was transferred into a Teflon lined autoclave (K. U. Leuven workshop) and placed in an oven for hydrothermal treatment at a temperature of 90 °C for another 48 h. Finally, the powder was washed on a 0.45 μm filter (Whatman Schleicher and Schuell) with demineralized water, dried and calcined at 550 °C for 8 h under ambient atmosphere to remove the triblock copolymer from the pores.

Itraconazole Loading of SBA-15. SBA-15 materials were loaded with itraconazole (Janssen Pharmaceutica) by the incipient wetness impregnation aiming at a drug content of 20 wt %. A concentrated solution of the drug in dichloromethane (20 mg in 400 μL) was prepared and added to 80 mg of SBA-15 material. During the addition of itraconazole solution, the powder was intensively mixed with a spatula. The powders were first dried at 35 °C in air for 24 h and subsequently placed under reduced pressure (1 hPa) at 40 °C for 48 h. In this way, itraconazole was loaded into the mesopores of SBA-15. Details of the physical state of adsorbed itraconazole have been published in earlier work.[9d]

Caco-2 Cell Monolayer Transport Experiments. Caco-2 cells were purchased from Cambrex Biosciences (Walkers-

(16) Rosenholm, J. M.; Peuhu, E.; Eriksson, J. E.; Sahlgren, C.; Linden, M. Targeted Intracellular Delivery of Hydrophobic Agents using Mesoporous Hybrid Silica Nanoparticles as Carrier Systems. *Nano Lett.* **2009**, *9*, 3308–3311.

(17) Tao, Z.; Morrow, M. P.; Asefa, T.; Sharma, K. K.; Duncan, C.; Anan, A.; Penefsky, H. S.; Goodisman, J.; Souid, A.-K. Mesoporous silica nanoparticles inhibit cellular respiration. *Nano Lett.* **2008**, *8*, 1517–1526.

(18) Lindfors, L.; Forssen, S.; Westergren, J.; Olsson, U. Nucleation and crystal growth in supersaturated solutions of a model drug. *J. Colloid Interface Sci.* **2008**, *325*, 404–413.

(19) Fatouros, D. G.; Walrand, I.; Bergenstahl, B.; Mullertz, A. Colloidal Structures in Media Simulating Intestinal Fed State Conditions with and Without Lipolysis Products. *Pharm. Res.* **2009**, *26*, 361–374.

ville, MD). Caco-2 cells were grown in 75 cm^2 culture flasks at 37 °C in an atmosphere of 5% CO_2 and 90% relative humidity. Cells were passaged every 3−4 days (at 70−80% confluence) at a split ratio of 1 to 7. Cells were negative for *Mycoplasma* infection. For transport experiments, Caco-2 cells were plated at a density of 100000 cells/insert on Costar Transwell membrane inserts (3 μm pore diameter, 12 mm diameter; Corning Inc.). Confluence was reached within 3−4 days after seeding, and the monolayers were used for the experiments 18−19 days postseeding. Cell passages between 50 and 85 were used in the experiments. Transepithelial electrical resistance values (TEER values) were measured with an EndOhm voltohmmeter (WPI). Only monolayers with initial TEER values higher than 200 $\Omega \cdot cm^2$ were used. All volumes amounted to 0.5 mL at the apical side of the monolayer and 1.5 mL at the basolateral side. After rinsing the monolayers 3 times with TM, a preincubation step (30 min) with TM (control) was performed.

After measuring TEER values, transport was initiated by adding to the donor compartment: (a) a crystalline itraconazole suspension in FaSSIF and (b) a suspension of SBA-15 loaded with itraconazole in FaSSIF. Samples (100 μL) were taken from the acceptor compartment after 30, 60, and 90 min and replaced with 100 μL of fresh receiver medium. During the experiments, 0.2% TPGS was included in the TM added to the basolateral compartment to install sink conditions. The samples were diluted with methanol (1:1), and itraconazole concentration was determined with HPLC-UV. The HPLC system (Merck-Hitachi) used consisted of an Elite LaChrom L-2130 HPLC pump, an autosampler model L-2200 and a UV detector model L-2400. The separation of itraconazole was performed on an RP-18 150 4.6 mm 5 μm Hypersil silica column (Thermo Electron Corporation) at room temperature. The mobile phase consisted of acetonitrile:tetrabutyl ammonium hydrogen sulfate 0.01 N (55:45 v/v), and was filtered through a 0.45 μm PTFE membrane and degassed by ultrasonication before use. The flow rate amounted to 1.5 $mL \cdot min^{-1}$, and the effluent was monitored at a wavelength of 265 nm. TEER values were measured again at the end of the experiment and were higher than 95% of the initial value. As an additional control of the monolayer integrity, sodium fluorescein flux was measured at the end of the experiment. Briefly, sodium fluorescein (1 $mg \cdot mL^{-1}$) was added to the apical compartment, and after 60 min, samples were taken from the basolateral compartment, followed by TEER measurement. The amount of sodium fluorescein appearing in the basolateral compartment was measured by UV spectrophotometry (Uvikon 810P spectrofotometer, Kontron Instruments) at 490 nm. Sodium fluorescein flux values across the monolayers were below $0.6\% \cdot h^{-1} \cdot cm^{-2}$. None of the test conditions affected the integrity of the tight junctions during the time period studied (based on TEER measurements and sodium fluorescein flux).

Cryogenic Transmission Electron Microscopy (Cryo-TEM). The sample vitrification procedure was carried out using an automated vitrification robot (FEI Vitrobot Mark III) equipped with humidity and temperature controlled glovebox. Prior to the vitrification procedure the cryo-TEM grids (R2/2 Quantifoil Jena) were surface plasma treated using a Cressington 208 carbon coater. The cryo-TEM experiments were on the TU/e CryoTitan (FEI) with an autoloader (http://www.cryotem.nl). The TU/e CryoTitan is equipped with a field emission gun (FEG) operating at 300 kV. Images were recorded using a 2k × 2k Gatan CCD camera equipped with a post column Gatan Energy Filter (GIF).

Electron Spin Resonance (ESR). The spectra were recorded in a Bruker flat cell at room temperature using a Bruker ESP300E. The spectrometer settings were as follows: modulation frequency, 100 kHz; modulation amplitude, 1.0 G; microwave power, 8 mW; scan range, 80 G; scan rate, 1 G/s; time constant, 20.48 s. Rotational correlation times were calculated from the ESR spectra using the expression by Cannon et al.: $\tau = 6.5 \times 10^{-10} W_0 \{[h_0/(h_{-1})]^{1/2} + (h_0/h_{+1})^{1/2} - 2\}$, where W_0 is the peak-to-peak line width of the middle field line and h_0, h_{-1} and h_{+1} are the peak-to-peak heights of the mid-, high- and low-field lines, respectively.

Dynamic Light Scattering (DLS). DLS was performed with an ALV CGS-3 multiangle goniometer with a HeNe laser having a wavelength of 632.8 nm with 22 mW output power. Samples were measured at 25.0 °C. The intensity autocorrelation function was measured at different scattering angles between 30 and 150° during 30 s each.

Results and Discussion

Cryogenic Transmission Electron Microscopy. Cryo-TEM was used to probe the structural characteristics of the supramolecular assemblies present in FaSSIF during the generation of itraconazole supersaturation with SBA-15 as SDDS. The advantage of cryo-TEM is that aqueous samples can be studied in their native environment without causing any destruction of the sample.[20] At different times during the release process as in Figure 1, FaSSIF containing itraconazole was separated from SBA-15 and frozen rapidly using liquid propane. In this way, the structures present during the first as well as the second phase could be investigated, by sampling after respectively 15 min (phase I), 180 min (phase II) and 24 h (phase II). The observations in cryo-TEM of these samples can now be compared with pure FaSSIF. Figure 2 presents the cryo-TEM images of pure FaSSIF (Figure 2A) and after itraconazole release for 15 min (Figure 2B). Both pictures display the mixed micelles (some are indicated by arrows) which consist of the bile salt taurocholate and lecithin. Their size measured by cryo-TEM is 12 nm. It should be noted that the darker spots present in Figures 2A and 2B are ice crystals that were formed during the sample preparation. This observation suggests that the solubilization of itraconazole with a concentration below 5 μM barely impacts the structural characteristics of the mixed

(20) Pouget, E. M.; Bomans, P. H. H.; Goos, J. A. C. M.; Frederik, P. M.; de With, G.; Sommerdijk, N. A. J. M. The Initial Stages of Template-Controlled CaCO3 Formation Revealed by Cryo-TEM. *Science* **2009**, *323*, 1455–1458.

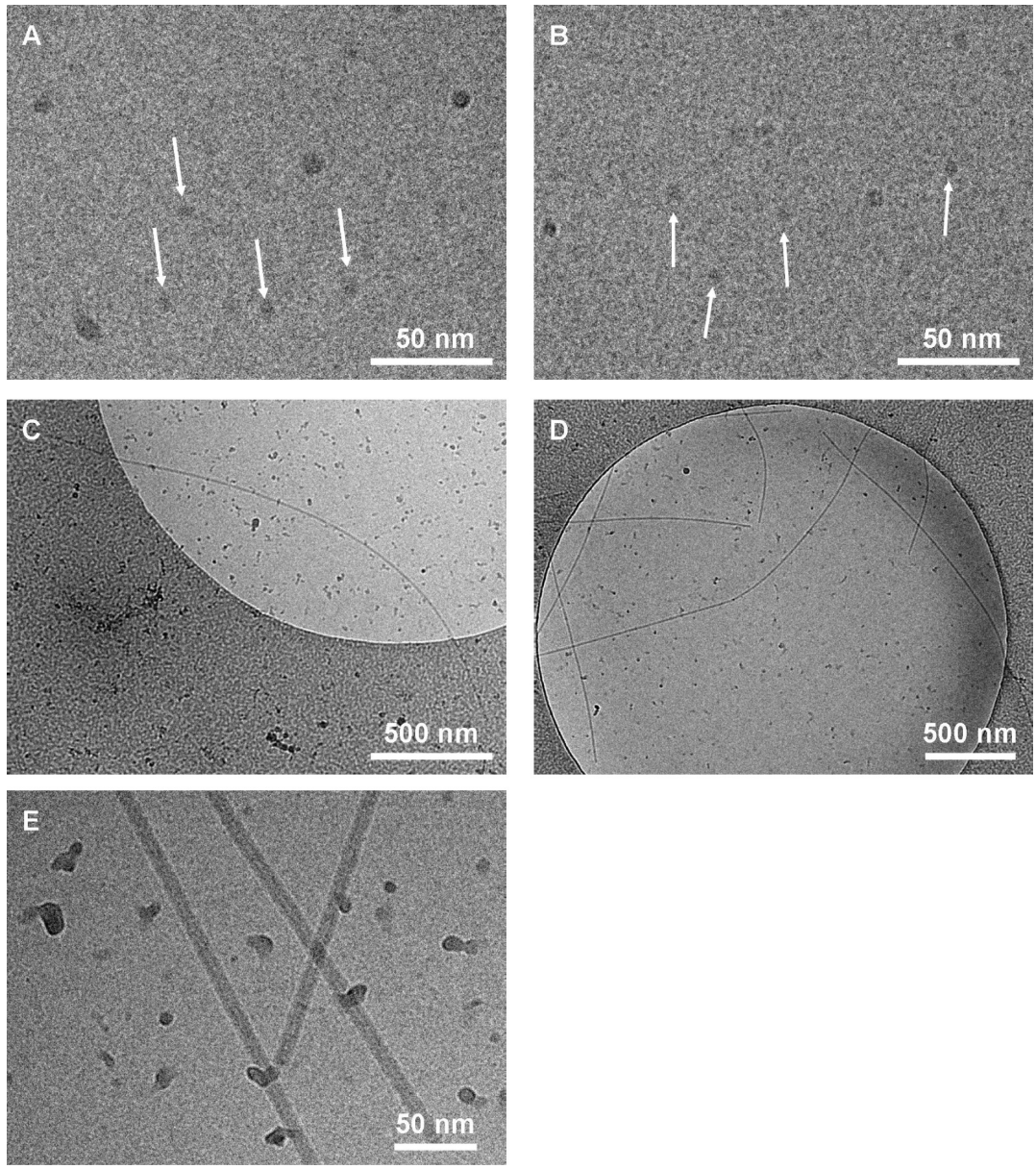

Figure 2. Cryo-TEM images of (A) pure FaSSIF and after itraconazole release from SBA-15 during (B) 15 min (arrows indicate some of the mixed micelles), (C) 180 min and (D) 24 h. (E) Detail of the observed nanofibers.

micelles in FaSSIF. The second phase of the itraconazole release from SBA-15 in FaSSIF is characterized by a drastically increasing amount of liberated itraconazole. Until now, the underlying mechanism for this enhancement remained unclear.[13] Figure 2 presents cryo-TEM images of FaSSIF after itraconazole release for 180 min (Figure 2C) and 24 h (Figure 2D). Both pictures reveal the presence of relatively long, but very thin fibers. The length and concentration of these nanofibers apparently increase with time. The nanofibers have a uniform diameter of 12 nm and display lengths up to several micrometers. Figure 2E presents a detailed cryo-TEM picture of these nanofibers.

Caco-2 Cell Monolayer Transport Experiments. The contribution of itraconazole in the formation of the nanofibers can be verified by studying the transepithelial transport across a Caco-2 cell monolayer. The Caco-2 system is derived from colon carcinoma cells and mimics the polarized absorptive epithelium of the small intestine. This bicompartimental Caco-2 system has proven to be ideal for intestinal absorption simulations and has become an industry standard for the investigation of intestinal absorption, permeability and drug−drug interactions.[21] Figure 3 presents the total amount of itraconazole appearing at the basolateral side after transepithelial transport as a function of time. The apical compartment contained SBA-15 loaded with itraconazole suspended in FaSSIF. The fraction of itraconazole liberated from SBA-15 already was presented in Figure 1. We allowed itraconazole release from SBA-15 during 15, 30, and 90 min

(21) Press, B.; Di Grandi, D. Permeability for Intestinal Absorption: Caco-2 Assay and Related Issues. *Curr. Drug Metab.* **2008**, *9*, 893–900.

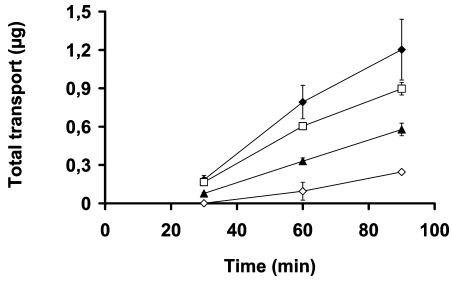

Figure 3. Total transport (μg) of itraconazole as a function of time across a Caco-2 cell monolayer. Donor media: SBA-15 suspension with a theoretical itraconazole concentration of 75 μM in FaSSIF. Transport is initiated following a prerelease of itraconazole from SBA-15 in FaSSIF during 0 min (◆), 15 min (□), 30 min (▲) and 90 min (◇).

to increase the liberated fraction itraconazole before initiating transepithelial transport. When transepithelial transport was initiated immediately after making the suspension, total transport after 90 min amounted to 1.20 ± 0.24 μg. When prerelease was respected, total itraconazole transport across a Caco-2 cell monolayer after 90 min was decreased to 0.90 ± 0.05 μg, 0.58 ± 0.05 μg and 0.25 ± 0.01 μg as presented in Figure 3. This observation is opposite to what could be expected from Fick's law, assuming that the concentration of itraconazole is increased by prerelease. As the diffusive process is passive, an increased apical concentration should result in an increased transepithelial transport. Diffusion through Caco-2 cells, however, only takes place when itraconazole is present in a dissolved state. The observation that a decreased transepithelial transport is measured, combined with increased amount of released itraconazole on the apical side, evidence that the itraconazole molecules were not freely available. The presence of nanofibers as observed in cryo-TEM rationalizes this observation, and suggests that these nanofibers are made up of itraconazole. Due to the nature of the Caco-2 system, such large supramolecular assemblies of itraconazole cannot be transported through a Caco-2 cell monolayer. The nanofiber morphology has not been observed before. Pure crystalline itraconazole typically is composed of large irregular crystals with a broad size distribution.[22] However, fine needles have been observed for novel engineered cocrystals of itraconazole and fumaric acid or tartaric acid.[23]

Electron Spin Resonance. The formation mechanism of the nanofibers was investigated further with ESR by probing the exact localization of itraconazole in the micellar system of FaSSIF during the progressive release

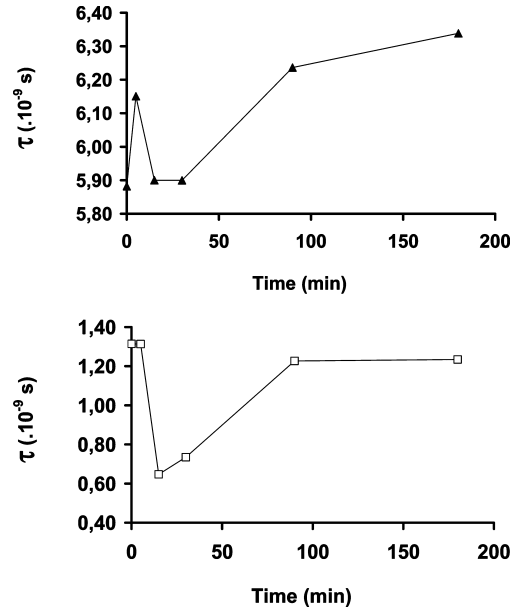

Figure 4. Rotational correlation times (τ) of spin probes 5-doxylstearic acid (▲) and 16-doxylstearic acid (□) determined with ESR and presented as a function of time during the release of itraconazole from SBA-15 in FaSSIF.

from SBA-15. We used two different doxylstearic acid probes which contain their nitroxide paramagnetic center at the C5 or C16 position. The amphiphilic nature of stearic acid ensures the positioning in the micelles, while the different position of the nitroxide group allowed us to probe the environment at different depths in the micelle. The nitroxide groups of 5- and 16-doxylstearic acid are respectively located near the micelle/water interphase and orientated somewhat deeper toward the hydrophobic core of the micelle. The rotational correlation times (τ) of 5- and 16-doxylstearic acid at different times during itraconazole release from SBA-15 are presented in Figure 4. The time scale during generation of itraconazole supersaturation using SBA-15 as a SDDS was exactly the same as presented in Figure 1. The τ values for 5- and 16-doxylstearic acid at time zero amounted to 5.88×10^{-9} s and 1.31×10^{-9} s, respectively. The difference is attributed to the different localization of the nitroxide group in the micelles. The larger rotational correlation time of 5-doxylstearic acid indicates that the probe is more immobile when its nitroxide group is localized closer to the polar regions of the mixed micelles. The τ value obtained for 5-doxylstearic acid is ca. 5 times larger than those encountered in previous studies of simple bile salt micelles.[24] This can be attributed to the presence of lecithin in addition to the bile salt taurocholate in the mixed micelles of FaSSIF. Lecithin contains a negatively charged phosphate group that strongly interacts with the

(22) Lee, S.; Nam, K.; Kim, M. S.; Jun, S. W.; Park, J. S.; Woo, J. S.; Hwang, S. J. Preparation and characterization of solid dispersions of itraconazole by using aerosol solvent extraction system for improvement in drug solubility and bioavailability. *Arch. Pharm. Res.* **2005**, *28*, 866–874.

(23) Remenar, J. F.; Morissette, S. L.; Peterson, M. L.; Moulton, B.; MacPhee, J. M.; Guzman, H. R.; Almarsson, O. Crystal engineering of novel cocrystals of a triazole drug with 1,4-dicarboxylic acids. *J. Am. Chem. Soc.* **2003**, *125*, 8456–8457.

(24) Reis, S.; Moutinho, C. G.; Pereira, E.; de Castro, B.; Gameiro, P.; Lima, J. L. F. C. beta-Blockers and benzodiazepines location in SDS and bile salt micellar systems—An ESR study. *J. Pharm. Biomed. Anal.* **2007**, *45*, 62–69.

nitroxide group of 5-doxylstearic acid causing a seriously reduced mobility of the probe. The τ value of 16-doxylstearic acid in our system of mixed micelles is also slightly higher than those encountered with simple bile salt micelles reported before. Kawamura et al. proposed that the stearic acid probe penetrates through a simple bile salt micelle because of its small size.[25] The molecular length of stearic acid is estimated at 2.6 nm and exceeds the diameter of simple bile salt micelles which has been reported to vary between 1.5 and 2 nm. Cryo-TEM evidenced that the diameter of the mixed micelles encountered in FaSSIF is much larger than the diameter of simple bile salt micelles. This causes the nitroxide group of 16-doxylstearic acid to reside in more hydrophobic regions somewhat closer to the core the micelles instead of projected toward the exterior as in the case of simple bile salt micelles. The mobility of the probe therefore will be reduced and the rotational correlation time slightly increased in the present study. Figure 4 clearly illustrates that the release and subsequent solubilization of itraconazole has a strong influence on the rotational correlation times of both probes at different times. It can be assumed that alterations of the τ values result from a change in chemical environment of the probe caused by itraconazole positioning inside the micelles of FaSSIF. During the first phase of itraconazole release, the τ value of 5-doxylstearic acid increased from 5.88×10^{-9} s to 6.15×10^{-9} s after 5 min and dropped again to 5.90×10^{-9} s after 15 and 30 min. The τ value of 16-doxylstearic acid was altered exactly at the opposite time intervals when compared to 5-doxylstearic acid. After 5 min the τ value remained unchanged at 1.31×10^{-9} s, but decreased to 6.47×10^{-10} s and 7.35×10^{-10} s after 15 and 30 min, respectively. These observations suggest that the uptake of itraconazole toward the inside of the hydrophobic core of the mixed micelles of FaSSIF takes place during the first 30 min of the release process. The position of the nitroxide group close to the surface and deeper toward the hydrophobic core for 5- and 16-doxylstearic acid reveals that the itraconazole molecules are localized close to the micelle surface after 5 min. Itraconazole migrates deeper toward the hydrophobic core of the micelles as evidenced by the decreased τ value of 16-doxylstearic acid after 15 and 30 min. This micellar solubilization of itraconazole coincides with the first phase of itraconazole release presented in Figure 1. It can be assumed that itraconazole is released from SBA-15 during the first 10 min until the maximum attainable degree of supersaturation is reached. Hereafter, the release is interrupted because there is no more driving force to liberate the itraconazole molecules from the nanostructured void space of SBA-15. The time period between 10 and 30 min is therefore characterized by a fairly constant itraconazole concentration and involves the migration of the dissolved itraconazole fraction from the exterior toward the interior of the mixed micelles. This increased itraconazole concentration inside the mixed micelles probably initiates the formation of the nanofibers observed by cryo-TEM. It is striking that the size of the mixed micelles observed in cryo-TEM agrees with the width of 12 nm of the nanofibers. The continuing aggregation process subsequently generates a driving force for itraconazole release from SBA-15. This second phase characterized by a steep rise in liberated amount of itraconazole was also investigated with ESR using 5- and 16-doxylstearic acid as spin probes. The τ value of 5-doxylstearic acid increased from 5.90×10^{-9} s to 6.24×10^{-9} s and 6.34×10^{-9} s after respectively 90 and 180 min, while the τ value of 16-doxylstearic acid remained fairly constant when compared to its original value observed in pure FaSSIF. This indicates that itraconazole molecules released from SBA-15 directly participate to the growth of the nanofibers. The deeper regions of the mixed micelles remain unaffected during the second phase of itraconazole release from SBA-15.

Dynamic Light Scattering. The growth of the nanofibers was investigated using DLS. From the correlation function, the hydrodynamic diameter of the mixed micelles composed out of lecithin and the bile salt taurocholate in pure FaSSIF was determined at 27.2 ± 0.3 nm using the Stokes−Einstein relationship. This value is approximately twice as large as the 12 nm diameter observed with cryo-TEM. The hydrodynamic diameter obtained with DLS represents the micelle size together with a solvated water shell associated with the polar head groups at the micelle surface during diffusion. Cryo-TEM provides a phase contrast between the mixed micelles and the frozen aqueous solvent and measures the core diameter instead of a hydrodynamic diameter. The solvated water layer and possible electroviscous effects cause the diameter obtained by DLS to be larger compared to the one obtained with

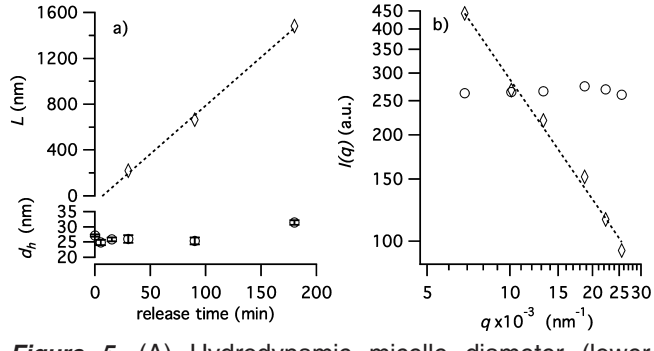

Figure 5. (A) Hydrodynamic micelle diameter (lower part), with error bars representing one standard deviation, and fiber diameter (upper part), at different times during release of itraconazole from SBA-15. The dotted line is a linear fit to the nanofiber length. (B) Static intensity of micelles (○) and nanofibers (◊) as a function of the scattering vector q, after 180 min release time. The dotted line is a power law fit to the nanofiber intensity, having an exponent of 1.13 ± 0.05.

(25) Kawamura, H.; Murata, Y.; Yamaguchi, T.; Igimi, H.; Tanaka, M.; Sugihara, G.; Kratohvil, J. P. Spin-label studies of bile salt micelles. *J. Phys. Chem.* **1989**, *93*, 3321–3326.

Scheme 1[a]

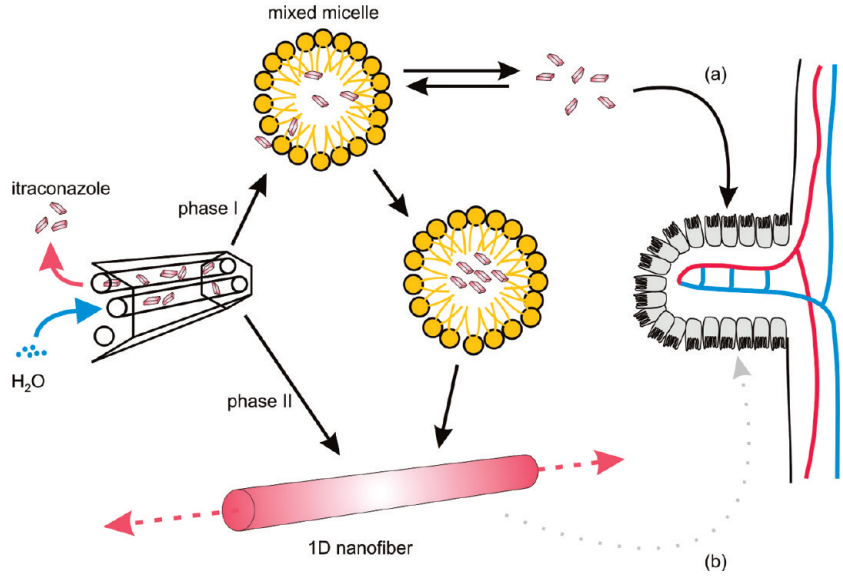

[a] Phase I: Itraconazole is released from SBA-15 and solubilized inside the mixed micelles of FaSSIF. The supersaturated state of itraconazole enhances transepithelial transport (a). Phase II: Itraconazole aggregates into nanofibers that grow in 1 dimension. This growth is a driving force for liberating itraconazole from the SBA-15 void space. Nanofibers can not be transported across an epithelial cell monolayer (b).

cryo-TEM.[26] For samples which had been prereleased and which correspond to phase 2, a second relaxation in the DLS correlation function was observed, which could be attributed to the nanofibers exhibiting their own characteristic diffusion. The length of the nanofibers as well as the hydrodynamic diameter of the mixed micelles as a function of time during the release of itraconazole from SBA-15 in FaSSIF is presented in Figure 5A. The full DLS results and details of the method used to determine the nanofiber length are provided as Supporting Information. The size of the mixed micelles remains almost constant during the release process, indicating that the introduction of itraconazole into the medium FaSSIF has no profound impact on the structure of the mixed micelles. Figure 5A clearly illustrates that the nanofiber length increases as a function of time. A length of 220 nm was observed after 30 min, and this value increases to 670 and 1480 nm, after 90 and 180 min respectively. The nanofiber growth process is very peculiar as it proceeds in one single dimension while the nanofiber width remains constant. The similar size of the mixed micelles and the nanofiber diameter observed in cryo-TEM suggests that the nanofiber formation begins inside the mixed micelles. Linear extrapolation of the growth curve from Figure 5A to a nanofiber length equal to zero yields a time equal to 7 min, which compares well to the time at which the maximum degree of itraconazole supersaturation is attained during the first phase of itraconazole release. This corroborates the conclusion obtained with ESR that nanofiber formation is initiated from the supersaturated state of itraconazole inside the micelles.

In the light scattering experiments, the angular dependency of total scattered intensity could be used to further asses the shape of the nanofibers in the liquid state. Figure 5B shows the static intensity of micelles and fibers after 180 min of release. Here, the scattering angle is expressed in terms of the scattering vector $q = 4\pi n \sin(q)/\lambda$, where n is the solvent refractive index and λ is the wavelength of the incident laser. The intensity of micelles was almost constant over the studied q-range (Figure 5B) because the micelle size was significantly smaller than $2\pi q^{-1}$, the length scale probed in the scattering experiment. On the other hand, the intensity of fibers showed power law decay with an exponent of -1.13 ± 0.05 (fitted curve in Figure 5B). This exponent is close to the theoretical value of -1 for perfectly rigid fibers. This observation confirms the 1D morphology of the fibers and shows that the fibers are rather rigid, in agreement with the cryo-TEM observations.

Conclusion

In summary, we elucidated the physical state of itraconazole in FaSSIF under conditions corresponding to supersaturation. Ordered mesoporous SBA-15 silica carrier was used as SDDS. ESR revealed that during supersaturation, itraconazole molecules are solubilized inside the hydrophobic core of mixed micelles present in FaSSIF. The supersaturated state of itraconazole subsequently provoked the formation of nanofibers exhibiting a width of 12 nm. The length of these nanofibers increased from 220 to 1480 nm after 30 and 90 min release from SBA-

(26) (a) Loftsson, T.; Brewster, M. E. Physicochemical properties of water and its effect on drug delivery—A commentary. *Int. J. Pharm.* **2008**, *354*, 248–254. (b) Russel, W. B.; Saville, D. A.; Schowalter, W. R. *Colloidal dispersions*; Cambridge University Press: Cambridge, 1989.

15, respectively. The participation of itraconazole in the formation of these nanofibers prevents its transepithelial transport across a Caco-2 cell monolayer which mimicks the gastrointestinal barrier. Based on our study, we suggest the existence of an optimum intraluminal itraconazole supersaturation at which itraconazole absorption is enhanced but formation of itraconazole nanofibers prevented (Scheme 1).

Acknowledgment. We are grateful to P. H. H. Bomans and N. A. J. M. Sommerdijk of TU/e for cryo-TEM investigations (http://www.cryotem.nl). R.M. and A.A. acknowledge the Flemish FWO for a postdoctoral fellowship. J.A.M. acknowledges the Flemish government for long term structural funding (Methusalem) and for supporting a Concerted Research Action (GOA). The topic of controlled release is investigated in Interuniversity Attraction Poles (IAP-PAI).

Supporting Information Available: (i) Full DLS results, (ii) details of the determination of the nanofiber length, (iii) Caco-2 data obtained with DMSO-shift method. This material is available free of charge via the Internet at http://pubs.acs.org.

MP900300J